Supplementary Information (SI) for Journal of Materials Chemistry C.
This journal is © The Royal Society of Chemistry 2026

# Supplemental Material For

## Non-parametric Statistical Characterization of Electrical Characteristics in Nanoscale Conductive Filament Devices

**ABSTRACT** This document serves as supplementary material for the paper "Non-Parametric Statistical Characterization of Electrical Characteristics in Nanoscale Conductive Filament Devices." It details experimental data for Ag, Ni, and Co conductive filament devices as well as VCM devices, which are not covered in the main text. The analysis includes calculations of the 50th percentile and its confidence intervals, quartiles, and IQR for these devices, alongside the Cu conductive filament devices discussed in the main text. Finally, it calculates some parameters for flash memory devices to support the comparative analysis between the two technologies outlined in the main text.

### 1. Introduction

This material provides supporting information for the calculations and discussions presented in the main text. Due to space constraints and to ensure a coherent narrative in the main text, only the dataset for Cu conductive filament devices is presented there. This supplemental document provides the corresponding data for Ag, Co, and Ni conductive filament devices, as well as for the valence change mechanism (VCM) devices discussed. After describing the non-parametric statistical methods employed, we report the 50th percentile confidence intervals, quartiles, and interquartile ranges (IQR) for all device types. Finally, we establish benchmark values for the Flash memory devices discussed in the main text.

### 2. Experimental data for Ag, Ni, and Co conductive filament devices and VCM devices

This section contains Tables S1–S3 as follows: Ag conductive filament device data (Table S1), Ni and Co conductive filament device data (Table S2), and VCM device data (Table S3). All parameter definitions are consistent with those in the main text and are not repeated here.

Table S1. Characteristics of the Ag conductive filament devices

| Structure and switching layer | MW /$R_{LRS}$ | $V_F$(V) /$V_{Read}$ | $V_{Set}$(V) /$I_{Setmax}$ | $V_{Reset}$(V) /$I_{Resetmax}$ | Write pulse | Erase pulse | Retention(s) Endurance（cycles） | Year /Ref. |
|---|---|---|---|---|---|---|---|---|
| B:Ag/$Ge_{0.3}Se_{0.7}$/Ti/Pt (Ag):50nm/NS | $10^5$ /1kΩ | 0.35 /NS | 0.22V /1nA | －0.06 /1nA | 100μA | 100μA | NS /NS | 2007 /[1] |
| B:Ag/ZnO:Mn/Pt (Ag):30nm/NS | $10^8$ /0.03 kΩ | NO /0.1V | 0.6 /5mA | –0.22 /5mA | 3V5mA 5ns | –3V5mA 5ns | $10^7$/100 | 2009 /[2] |
| B:Ag/$SiO_2$/Pt (Ag):7nm/NS | $10^3$ /1 kΩ | 0.8 /0.1V | 0.25 /0.15mA | －0.08 /0.15mA | / | / | $10^3$ /500 | 2012 /[3] |

| | | | | | | | | |
|---|---|---|---|---|---|---|---|---|
| B:Ag/$SiO_2$/$Ta_2O_5$/Pt (Ag):6.5nm/NS | $10^3$ /1 kΩ | NO /0.1V | 0.14~ 0.24 /0.15mA | －0.06 ~–0.14 /0.15mA | 1.2V 1ms | –1V 1ms | $10^5$/$10^3$ | 2012 /[3] |
| B:Ag/$Ta_2O_5$/Pt (Ag):15nm/NS | 100 /1 kΩ | 0.5 /0.1 | 0.2 /0.15mA | –0.1 /0.15mA | / | / | NS/500 | 2020 /[3] |
| B:Ag/$SiO_2$/ITO (Ag):60nm/NS | 100 /0.1 kΩ | NO /0.1V | 3 /1mA | –2 /1mA | 5V200μA 100ns | –10 V 250μA 100ns | 2×$10^3$ /500 | 2014 /[4] |
| B:Pt/ $Ag_xTe_{1-x}$/$Al_2O_3$/Si (Ag):20nm/ 5bits | 1.8×$10^3$/0 .4 kΩ | 2 /0.1V | ~1 /1mA | –0.5 /2mA | / | / | NS/500 | 2015 /[5] |
| B:TiN/Ag/CuO/TiN (Ag)：25nm/4bits | 127 /0.5 kΩ | NS /0.1V | 0.96 /1mA | –1.5 /1mA | 3V1mA 100μs | –2V1mA 100μs | NS/$10^5$ | 2015 /[6] |
| B:Ag/a-ZnO/Pt (Ag):100nm/NS | $10^7$ /1 kΩ | NO /0.1V | 0.15~ 0.45 /0.5m A | –0.23 /0.8m A | 3V 20ns 1mA | –3V 300ns 1 mA | $10^7$/100 | 2016 /[7]] |
| B:Ag/$NiO_x$/$TiO_2$/FTO (Ag+Ni):100nm/NS | $10^3$ /0.8 kΩ | NS /0.2V | 2 /10mA | –1.8 /12mA | / | / | $10^4$/100 | 2017 /[8] |
| B:Ag/$SiO_2$/TiN (Ag):36nm/NS | 10 /1 kΩ | –5.5V /0.1V | –1.1 /~7mA | ~0.75 /~7mA | / | / | $10^4$(358K) /100 | 2018 /[9] |
| B:Ag/$ZrO_2$/$WS_2$/Pt (Ag):100nm/NS | $10^6$ /0.1 kΩ | 0.5V /NS | 0.16 /0.5mA | –0.06 /–0.2mA | 0.8V 100ns 3mA | –2.5V 100ns 1.5mA | $10^4$(363K) /$10^9$ | 2018 /[10] |
| B:Ag/$HfO_x$:N(2sccm)/Pt (Ag):50nm/NS | 5×$10^8$ /1 kΩ | NS/ 0.1V | 0.2 /0.1mA | ~0.07 /40μA | 2V 50μs 0.1mA | –0.25V 5μs 10μA | NS/$10^6$ | 2019 /[11] |
| B:Ag/$SiO_2$/Pt (Ag):20nm/NS | 2.68×$10^4$ /209 Ω | 2.35 /NS | 0.86 /1mA | －0.67 /3mA | / | / | NS/100 | 2019 /[12] |
| B:Ag/$Ge_{3.5}Sb_{1.0}Te_{5.5}$/TiN (Ag):200nm/2bits | 500 /0.1 kΩ | 1V /0.1V | 0.5 /0.1mA | 0.1V /0.03mA | / | / | $10^4$/100 | 2019 /[13] |
| B:Ag/a-BN/Pt (Ag):5.5nm/NS | 15 /0.4 kΩ | NS /0.2V | 0.4 /1mA | –0.45 /1mA | 1V1mA 50μs | –1.9V1mA 50μs | $10^4$/$10^4$ | 2019 /[14] |
| B:Ag/a-BN/Pt (Ag):21.5nm/NS | 2×$10^4$ /667Ω | 2.8 /0.2V | 0.6 /1mA | –0.4 /1mA | 1V1mA 500μs | –4.5V1mA 500μs | $10^4$/$10^4$ | 2019 /[14] |
| B:Ag/$SiO_2$:Ag/$TiO_2$ /p++ Si;(Ag):105.8nm/NS | 60/ 0.167 kΩ | NS /0.5V | 1.8 /5mA | –3.5 /5mA | / | / | $10^5$/$10^3$ | 2020 /[15] |
| B:Ag/DMcT-cc/$TiO_2$NP/ FTO;(Ag):359nm/NS | $10^4$ /0.25 kΩ | NS /0.1V | –1 /10mA | 1 /0.7mA | / | / | 2×$10^4$ /NS | 2020 /[16] |
| B:Ag/$SnO_2$/Pt (Ag):20nm/NS | $10^3$ /0.1 kΩ | NS/0.1 V1μs | 0.15 /5mA | –0.25 /5mA | 1V50μs 5mA | –1V 50μs 5mA | 2×$10^4$ /$10^4$ | 2020 /[17] |
| B: Ag/ $SnO_2$/IGZO/Pt (Ag):20nm/NS | $10^3$ /17Ω | NS /0.05V | 0.06 /5mA | －0.1 /5mA | 0.6V 5mA 50μs | –0.6V 5mA 50μs | 2×$10^4$ /$10^5$ | 2020 /[17] |

| | | | | | | | | |
|---|---|---|---|---|---|---|---|---|
| U:Ag/IGZO/ $SnO_2$ /Pt<br>(Ag):20nm/NS | $10^3$<br>/50Ω | NS<br>/0.25V | ±1.5V<br>/5mA | ±0.75V<br>/5mA | ±2V<br>50μs5mA | ±1V<br>50μs5mA | 2×$10^4$<br>/$10^5$ | 2020<br>/[17] |
| B:Al/Ag/$Al_2O_3$/TiN<br>(Ag):20nm/NS | 6~8<br>/1 kΩ | 3.6<br>/0.1 | 1.5<br>/ 5mA | –0.4<br>/ 1mA | / | / | 3×$10^3$<br>/$10^3$ | 2020<br>/[18] |
| B:Al/Ag/$Al_2O_3$/TiN<br>(Ag):5nm/NS | $10^8$<br>/1~3 kΩ | 1.75<br>/0.1 | 0.8<br>/5mA | –0..4<br>/1mA | 1.5V 500μs<br>1mA | –0.12 V<br>500μs 5mA | 3×$10^3$<br>/$10^3$ | 2020<br>/[18] |
| B:Ag/MXene/$SiO_2$/Pt<br>(Ag):130nm/NS | $10^3$/<br>0.3 kΩ | >0.2<br>/0.01V | 0.2<br>/1mA | –0.2<br>/1mA | / | / | $10^4$<br>/100 | 2020<br>/[19] |
| B:Ag/NiO/ITO/PET<br>（Ag）:30nm/5bits | 100<br>/0.5 kΩ | NO<br>/0.1V | 0.75<br>/1mA | –1.23<br>/0.1mA | / | / | $10^5$<br>/100 | 2021<br>/[20] |
| B:Ag/$HfO_2$/Pt<br>(Ag):4nm/NS | 100<br>/1 kΩ | 0.72/<br>0.05V | 0.15<br>/1mA | –0.15<br>/1mA | 2.5V 5μs<br>0.2mA | –1V 5μs<br>0.2mA | ~$10^5$(423K)<br>/$10^8$ | 2021<br>/[21] |
| U:Ag/GeSe/Pt<br>(Ag):47nm/4bits | 1150<br>/33Ω | NO<br>/0.1V | ±0.97<br>/20mA | ±0.67<br>/20mA | / | / | $10^5$/<br>$10^4$ | 2022<br>/[22] |
| B:Ag/GeSe/Pt<br>(Ag): 6nm/6bits | 3.9<br>/25Ω | NO/<br>0.05V | 0.5V<br>/20mA | －0.4V<br>/20mA | 0.5V<br>30 μs | －0.5V<br>30μs | 5×$10^4$<br>(358K)/ $10^4$ | 2022<br>/[22] |
| B:Ag/$Cu_xO$/$SiO_x$/n-Si<br>(Ag): 18nm/NS | $10^7$<br>/1.67 kΩ | 2.5<br>/1V | 2.0<br>/10mA | –3.0<br>/10mA | / | / | 2×$10^4$<br>/1.2×$10^4$ | 2022<br>/[23] |
| B:Ag/GeS/Pt<br>(Ag)：15nm/NS | 2×$10^7$/<br>0.266 kΩ | ~0.6<br>/0.05V | 0.24<br>/1mA | –0.66<br>/1mA | / | / | 5×$10^4$/<br>$10^4$ | 2023<br>/[24] |
| B:Ag/IGZO/Pt<br>(Ag)：20nm/NS | 8×$10^3$/<br>10.5Ω | 1.6<br>/0.05V | 1.0<br>/5mA | –0.8<br>/5mA | / | / | 2×$10^4$/<br>$10^4$ | 2023<br>/[24] |
| B:Ag/IGZO/GeS/Pt<br>(Ag)：20nm/NS | $10^6$/<br>6.8Ω | 0.6<br>/0.05V | 0.32<br>/10mA | –0.54<br>/50mA | 1V<br>400ns | –2V<br>400ns | $10^5$<br>(355K) /$10^7$ | 2023<br>/[24] |
| B:Ag/Ta/Ag/AIN/Pt<br>(Ag):10nm/NS | 10<br>/0.4 kΩ | NS<br>/0.2V | 0.8<br>/1mA | –1<br>/1mA | / | / | $10^4$/<br>100 | 2023<br>[25] |
| B:Ag/$Ta_2O_3$/Au<br>(Ag):50nm/NS | $10^6$<br>/0.3 kΩ | 1.78<br>/0.1V | 0.59<br>/1mA | –0.58<br>/10mA | / | / | $10^3$/<br>200 | 2023<br>/[26] |
| B:Ag/$Ta_2O_3$/$Al_2O_3$/Au<br>(Ag+Vo): 60nm/NS | $10^6$<br>/0.1 kΩ | 7<br>/0.1V | 0.83<br>/1mA | –0.64<br>/1mA | / | / | $10^4$/<br>700 | 2023<br>/[26] |
| B:Ag/$VO_x$/Pt<br>(Ag):35nm/NS | 100<br>/0.1 kΩ | NO<br>/0.05V | 0.23V<br>/1mA | –0.07<br>/0.5mA | 1.5V 1mA<br>10 μs | –2V 1mA<br>10 μs | 4×$10^4$/<br>8000 | 2024<br>/[27] |
| B:Ag/$SiO_2$/TiN<br>(Ag):20nm/NS | 400<br>/0.5 kΩ | NS<br>/NS | 1.1V<br>/100μA | –0.1V<br>/100μA | 2.5V<br>500ns | / | 3.6×$10^5$<br>/50 | 2024<br>/[28] |
| B:Ag/ $ZrO_2$/ITO<br>(Ag):25nm/NS | $10^6$<br>/~2 kΩ | 4.7<br>/0.2 | 0.71<br>/0.1mA | –0.991<br>/0.3mA | / | / | / | 2024<br>/[29] |
| B:Ag/GeSe/$ZrO_2$/ITO<br>(Ag):50nm | $10^7$<br>/3 kΩ | 2.5<br>/0.2 | 0.54<br>/0.1mA | –0.47<br>/0.1mA | / | / | $10^4$/100 | 2024<br>/[29] |
| B:Ag/NiO/$ZrO_2$/ITO<br>(Ag):150nm/NS | $10^3$<br>/0.1 kΩ | NS<br>/0.1V | 2<br>/1mA | ~–0.4<br>/5mA | / | / | 3×$10^4$/<br>600 | 2024<br>/[30] |

Table S2. Characteristics of the Ni and Co conductive filament devices

| Structure and switching layer | MW /$R_{LRS}$ | $V_F$(V) /$V_{Read}$ | $V_{Set}$(V) /$I_{Setmax}$ | $V_{Reset}$(V) /$I_{Resetmax}$ | Write pulse | Erase pulse | Retention(s) /Endurance (cycles) | Year /Ref. |
|---|---|---|---|---|---|---|---|---|
| U:Ni/$HfO_x$/$AlO_y$/$SiO_x$ /$p^+$Si, (Ni):6.5nm/3bits | $10^5$ /0.9 kΩ | 3 /0.2V | >1.4 /0.1mA | >0.6 /1mA | >1.4V 0.1mA 10ns | >0.6V 1mA 30ns | $10^6$ /$10^6$ | 2011 /[31] |
| U:Ni/a-$HfO_x$ /$SiO_x$/$n^+$Si (Ni):4.4nm | $10^4$ /0.4 kΩ | 3 /NS | 2.1 /0.1mA | 1.1 /0.8mA | 3.8V, 3.8/ 0.5=7.6mA 50ns | 2.8V 50ns | $10^5$(423K) /$10^5$ | 2011 /[32] |
| U: Ni/$HfO_x$/p+Si (Ni):3nm | $10^3$ /<10 kΩ | NS /0.2V | 1. 5~2.4 /0.1mA | 1.5~1.9 /1mA | 1.5V 0.1mA 50ns | 2.1V 1mA 50ns | $10^5$(393K) /$10^3$ | 2011 /[33] |
| B:Ni/$TaO_x$/Ta/$TaO_x$/NiSi (Ni):22nm | $10^2$ /0.1kΩ | 4.42 /NS | 3 /10mA | –0.7 /10mA | / | / | NS /200 | 2012 /[34] |
| B: Ni/$HfO_2$/Pt (Ni):20nm | $8.2\times10^8$/ 196.86Ω | NO /0.1V | 5.12 /NS | –1.19 /NS | / | / | $10^3$ / NS | 2012 /[35] |
| U: Ni/$HfO_x$/n+Si (Ni):4nm | $10^3$ /2 kΩ | 3 /0.5V | 2.4 /0.1mA | 1.6 /1mA | / | / | $10^5$(423K) /$10^3$ | 2013 /[36] |
| B: Ni/$ZrO_2$/Pt (Ni):40nm | >!$0^6$ /0.1 kΩ | 9 /0.1V | 2 /10μA | –0.7 /10mA | / | / | / | 2013 /[37] |
| B: Ni/ZnO/Pt (Ni):90nm | 8.5/ 0.018 kΩ | 7.2 /0.1V | 0.9 /NS | –0.7 /NS | / | / | / | 2014 /[38] |
| B: Ni/ZnO/Ni (Ni):90nm | 13 /0.02 kΩ | 7.1 /0.1V | 1.1 /30mA | –0.6 /NS | / | / | $10^4$/20 | 2014 /[38] |
| U: Ni/$HfO_2$/$n^+$Si (Ni):20nm | $10^4$ /~8 kΩ | NS /0.8V | 3V /0.1mA | 0.8 /1mA | / | / | NS /2000 | 2014 /[39] |
| B:Au/Ni/$NH_3$treated $TaO_x$/NiSi (Ni):20nm | $10^4$ /0.01 kΩ | Yes /0.1V | 4.18 /10mA | –0.82 /10mA | / | / | $2\times10^4$ /100 | 2015 /[40] |
| B: Ni/$Ta_2O_5$/Si (Ni):13nm | $10^3$/ 0.167 kΩ | 6.2 /0.5 | 5.1V /NS | –2.8V /NS | 9V 0.2ms 12.5mA/ | –8V 0.2ms 10mA | $10^5$(360K) /$10^3$ | 2015 /[41] |
| U: Ni/a-$HfO_2$/Pt (Ni):4nm | NS/ 0.066 kΩ | NS /0.1V | 0.55 /4mA | –0.5 /4mA | / | / | NS /NS | 2015 /[42] |
| U: Ni/ $HfO_2$/Pt (Ni):10nm | 100 /1 kΩ | Yes /0.1V | 1.9 /0.1mA | 1.3 /1mA | / | / | NS /60 | 2015 /[43] |
| B: Ni/$HfO_x$/Pt (Ni):3.3nm | 8/0.3~ 0.4 kΩ | 0.7 /0.1V | 1 /1mA | –0.5 /1.6mA | / | / | NS /60 | 2015 /[44] |

| | | | | | | | | |
|---|---|---|---|---|---|---|---|---|
| B:Ag/$NiO_x$/$TiO_2$/FTO<br>(Ag+Ni):100nm | $10^3$<br>/0.8 kΩ | NS<br>/0.2V | 2<br>/10mA | –1.8<br>/12mA | / | / | $10^4$<br>/100 | 2017<br>/[8] |
| B:Au/Ni/TaON-$N_2$1.5<br>/NiSi, (Ni):20nm | $10^4$<br>/0.04 kΩ | Yes<br>/1V | 1.6~4<br>/10mA | –0.9~ –<br>1.5/10m<br>A | / | / | 5×$10^4$<br>/NS | 2018<br>/[3] |
| B: Pt/Cr/Ni/MgO/Ni<br>(Ni):10nm | >100<br>/50Ω | NO<br>/0.1V | 1.0<br>/12mA | –0.6<br>/12mA | / | / | $10^4$<br>/100 | 2019<br>/[45] |
| B: Ni/$SiO_2$/Pt<br>(Ni):30nm | >$10^3$<br>/0.1 kΩ | NO<br>/–0.2V | >3<br>/50μA | –0.5<br>/20mA | 3V 2μs<br>10mA | 2V 5μs<br>10.5mA | 2500<br>/50 | 2021<br>/[46] |
| B:Co/NiO/Pt<br>(Co):55nm | $10^2$~$10^3$<br>/0.1 kΩ | NS<br>/NS | 1.2<br>/10mA | –1<br>/10mA | / | / | NS<br>/100 | 2014<br>/[47] |
| U: Co/NiO/Pt<br>(Co):55nm | $10^2$~$10^3$<br>/0.1 kΩ | NS<br>/NS | –1.5<br>/10mA | –0.8<br>/20mA | / | / | NS<br>/100 | 2014<br>/[47] |
| B: Co/a-$HfO_2$/Pt<br>(Co):4nm | NS<br>/NS | NS<br>/NS | 2.3<br>/0.1mA | –1.4<br>/1mA | 6V25ns<br>/NS | / | NS<br>/NS | 2017<br>/[48] |
| B: Co/$HfO_2$/Pt<br>(Co):30nm | $10^3$<br>/0.4 kΩ | NS<br>/0.1V | 1<br>/0.1mA | –0.5V<br>/1mA | / | / | NS/$10^3$ | 2017<br>/[49] |
| B: Co/$Al_2O_3$/TiN<br>(Co):3nm | 3×$10^3$<br>/20 kΩ | 3.8<br>/NS | 2<br>/ 50μA | –1<br>/50μA | 3.5V<br>50μA<br>100ns | –1.3V<br>50μA<br>5μs | 3600<br>(458K)/$10^4$ | 2019<br>/[50] |
| B: Co/Ta/GeSe/TiN<br>(Co):23nm | ~$10^3$<br>/100 kΩ | 2.5<br>/0.1 | 3.5<br>/NS | –2<br>/NS | / | / | 3600<br>(458K)/$10^3$ | 2019<br>/[50] |
| B: Co/LaSiO/TiN<br>(Co):5nm | 200<br>/20 kΩ | Yes<br>/NS | 1.5<br>/0.1mA | –0.5<br>/0.1mA | 3.5V<br>50μA<br>100ns | –1.5V<br>50μA<br>100ns | 3600<br>(458K)/$10^7$ | 2020<br>/[51] |
| B: Pt/$Ta_2O_5$/$Co_{70}Cu_{30}$<br>(Co):7nm | 20/<br>0.6 kΩ | 2<br>/0.2V | 0.7<br>/1mA | –0.5<br>/1mA | 1.5V 70ns<br>2.5mA | –1.6 V<br>480ns<br>3mA | NS<br>/100 | 2023<br>/[52] |
| B: Pt/$Ta_2O_5$/Co<br>(Co):7nm | $10^2$<br>/0.7 kΩ | 2.3<br>/0.2V | 1.5<br>/1mA | –0.3<br>/1mA | 1.5V 130ns<br>2.5mA | –1.6V<br>920ns<br>2.5mA | NS<br>/100 | 2023<br>/[52] |
| B:W/Co/$SiO_x$/TiN<br>(Co):10nm | 100<br>/50K | 5<br>/NS | 2<br>/10μA | –2<br>/10μA | 8V 100ns<br>12.5mA | NS | $10^5$<br>/109 | 2023<br>/[53] |
| B: Co/HfSiO/W<br>(Co):3nm | $10^3$<br>/10 kΩ | 5<br>/–0.1 | 2.5<br>/0.05mA | –0.5<br>/0.2mA | / | / | NS<br>/$10^5$ | 2024<br>/[54] |
| B: Co/HfSiO/W<br>(Co):5nm | $10^3$<br>/10kΩ | 6.5<br>/–0.1 | 3.2<br>/0.05mA | –0.5<br>/0.2mA | 3.8V<br>50μA<br>200ns | –1.5V<br>50μA<br>8μs | NS<br>/$10^5$ | 2024<br>/[54] |
| B:Co/HfSiO/LaSiO/W<br>(Co):6~8nm | 100<br>/6 kΩ | NS<br>/NS | NS<br>/NS | NS<br>/NS | 4.2V<br>50μA<br>8μs | –1.6V<br>50μA<br>12μs | NS<br>/$10^5$ | 2024<br>/[54] |

| | | | | | | | | |
|---|---|---|---|---|---|---|---|---|
| B:Co/LaSiO /HfSiO/W (Co):6~8nm | $10^3$ /6 kΩ | NS /NS | NS NS | NS /NS | 3.7V 50μA 400ns | –0.8V 50μA 3μs | NS /$10^5$ | 2024 /[54] |

*The number of multilevel samples for Ni and Co filament devices is too small to be included in the statistics.

Table S3. Characteristics of the VCM devices

| Structure and switching layer | MW /$R_{LRS}$ | $V_F$(V) /$V_{Read}$ | $V_{Set}$(V) /$I_{Setmax}$ | $V_{Reset}$(V) /$I_{Resetmax}$ | Write pulse | Erase pulse | Retention(s) /Endurance (cycles) | Year /Ref. |
|---|---|---|---|---|---|---|---|---|
| U: Pt/ZnO/Pt (Vo):100nm /NS | $10^4$ /16Ω | 3.3 /0.1V | –2 /0.05A | –1 /0.03A | / | / | NS/>$10^2$ | 2008 /[55] |
| U: Al/$Al_xO_y$/Al (Vo):10nm /NS | ≥$10^4$ /33Ω | ～3.5 /0.1V | 2.3 /20mA | 0.4 /1μA | / | / | $10^4$(358K)/ ~$10^4$ | 2008 /[56] |
| B:Tin/ZnO/Pt (Vo):30nm/NS | 25 /0.2 kΩ | NO /0.5V 50ns | 1.2 /6mA | –0.6 /6mA | 4V4.5mA 10ns | –4V4.5mA 40ns | NS / NS | 2008 /[57] |
| B: Ti/$MnO_2$/Pt (Vo):80nm/NS | 50 /20Ω | NS /0.2V | 0.7 /5mA | –1.1 /5mA | 1.5V5mA 10ms | –1.5V5mA 10ms | >$10^4$(358K) />$10^5$ | 2009 /[58] |
| B: Ta/$TaO_x$/Pt (Vo) ~12nm/NS | ~10/ ~0.12 kΩ | 0.875 /NS | 0.6 /0.1mA | –0.6 /0.1mA | 1.9V 1μs | –2.2V 1μs | ~$10^7$/$10^9$ | 2010 /[59] |
| B: Au/ZnO/ITO (Vo):20nm/5bits | 330 /60Ω | NS /0.55V | –2 /20mA | 1.5 /35mA | / | / | $10^4$/ 120 | 2011 /[60] |
| B: Pt/ZnO/Pt (Vo):25nm/NS | 250 /0.2 kΩ | 4.0 /0.1V | 1.20 /3mA | –0.5 /3mA | 1.2V3mA 1ms | –0.9V3mA 1ms | $10^6$ /$10^6$ | 2012 /[61] |
| B:Ta/$TaO_x$/$TiO_2$/Ti (Vo):20nm/4bits | 20 /100 kΩ | NO/– 2V1μs | 5 /10nA | –4~–6 /70μA | 6V60μA 50ns | –5.5V60μA 50ns | >$10^4$ />$10^{12}$ | 2013 /[62] |
| B: Ni/$HfO_x$/$n^+$Ge (Vo):4nm/NS | $10^4$ /2 kΩ | 3.5 /0.5 | 2.5 /0.1mA | –1.5 /3mA | / | / | $10^4$/120 | 2013 /[63] |
| B: Al/$Ta_2O_5$/Pt (Vo):25nm/NS | 50 /0.8 kΩ | NS /NS | 0.8 /1mA | –1.1 /2mA | / | / | NS/100 | 2013 /[64] |
| B: Ti/$Ta_2O_5$/Pt (Vo):25nm/NS | 200 /0.5 kΩ | NS /NS | 1.0 /1mA | –1.2 /4mA | / | / | NS/100 | 2013 /[64] |
| B: Zr/$Ta_2O_5$/Pt (Vo):25nm/NS | 140 /0.5 kΩ | NS /NS | 3.2 /1mA | –2.4 /10mA | / | / | NS/100 | 2013 /[64] |
| B: TiN/$HfO_2$/Pt (Vo):24.7nm/NS | $10^6$ /1 kΩ | NO /0.5V | 6 /50μA | –3.5~ – 4/30μA | 200ns | –2.4 V 500ns 0.24m A | $10^4$(398K) /NS | 2014 /[65] |
| B: Pt/$AlO_\delta$/$Ta_2O_{5-x}$/$TaO_y$ /Pt, (Vo):56nm/4bits | $10^3$ /1 kΩ | –1.8 /0.1V | –1.2 /1mA | 1.9 /3mA | –1.9V 1mA 100ns | 2.3V 3mA 100ns | $10^4$(398K) /$10^{10}$ | 2014 /[66] |

| | | | | | | | | |
|---|---|---|---|---|---|---|---|---|
| U: Au/$ZnO_xS_{1-x}$/Al<br>$L_{ZnOxS1-x}$(Vo):40nm/NS | $10^6$<br>/~30Ω | Yes<br>/0.2V | 2.5<br>/1mA | 0.5<br>/30mA | / | / | $10^4$/100 | 2014<br>/[67] |
| B: W/Ta/$TaO_x$/Pt<br>(Vo): 7nm/3bits | ~$10^2$<br>/2.5 kΩ | 1/<br>0.2 V | 0.5～0.8<br>/30μA | –0.5<br>/200μA | / | / | >$10^4$(358K)<br>/>$10^8$ | 2015<br>/[68] |
| B:Ti/ $HfO_2$/$O_2$-$HfO_2$<br>/TiN, (Vo):10nm/NS | $10^3$<br>/1.5 kΩ | 5.5<br>/0.3V | 1<br>/0.5mA | –1<br>/0.5mA | 3.5V<br>0.5mA30ns | –3V 0.5mA<br>30ns | $10^4$(398K)<br>/$10^{10}$ | 2015<br>/[69] |
| B:Ti/$TiO_2$Np/$Ta_2O_5$/Au<br>(Vo):30nm/NS | 36<br>/17Ω | NO<br>/0.5V | 0.7<br>/100mA | –0.7<br>/100mA | / | / | NS/40 | 2015<br>[70] |
| B: Al/Al10%ZnO/Mo<br>(Vo):20nm/NS | 100<br>/0.15~<br>0.3kΩ | NS<br>/0.1V | 1.0<br>/10mA | –0.5<br>/0.5mA | 2V ~300μs<br>~5mA | –2V 0.7μs<br>~0.1mA | $10^4$<br>/100 | 2015<br>/[71] |
| B: ITO/a-$TiO_x$/AgNPs<br>/$TiO_x$/a-Al$TiO_x$/FTO<br>(Vo): 24nm/NS | 300<br>/16 kΩ | NO<br>/–0.1V | -0.36±<br>0.11<br>/20μA | 0.14±<br>0.07<br>/5μA | / | / | $10^4$<br>/>100 | 2016<br>/[72] |
| B: W/Ti/$TiO_x$/MgO/Ru<br>Ti$Ox$:3nm<br>(Vo):20+3nm | 21<br>/2 kΩ | NO<br>/0.3V | 0.87<br>/1mA | –0.9<br>/1mA | 1.4V<br>30ns | –1.8V<br>60ns | 3.5×$10^3$<br>/$10^9$ | 2016<br>/[73] |
| B: TiN/Ti/$TiO_{2-x}$/Pt NCs/<br>$TiO_{2-x}$ /Au,<br>(Vo):45nm/3bits | ~$10^5$<br>/10 kΩ | NO/<br>1V10m<br>s | 2<br>/0.2mA | –1.5<br>/0.2mA | 4V 0.2mA<br>100ns | –2.5V<br>0.2mA<br>100ns | $10^5$<br>/$10^5$ | 2016<br>/[74] |
| B: Pt/Ta$O_x$/Ta<br>(Vo):~35nm/3bits | 20<br>/2 kΩ | NO<br>/NS | 1<br>/1mA | –1<br>/1mA | 1.3V<br>200ns | –1.6V<br>500ns | ~$10^6$(423K)<br>/$10^8$ | 2016<br>/[75] |
| B: Al/$WO_3$/Pt<br>(Vo):170nm/NS | 30<br>/50Ω | ~3.2<br>/0.1V | 1<br>/30mA | –1<br>/30mA | 1.3V 100ns<br>6mA | –2V 140ns<br>6mA | 3×$10^4$<br>/200 | 2016<br>/[76] |
| B: Cu/$WO_3$/Pt<br>(Vo):170nm/NS | 10<br>/0.5 kΩ | ~3.7<br>/0.1V | 0.8<br>/3mA | –1.3<br>/3mA | 2V 150ns<br>0.32mA | –2 V 400ns<br>0.32mA | 3×$10^4$<br>/150 | 2016<br>/[76] |
| B: Pt/$WO_3$/Pt<br>(Vo):170nm/NS | 7<br>/14.3Ω | ~7<br>/0.1V | 1.7<br>/10mA | –2.2<br>/10mA | 2.5V 400ns<br>7mA | –2V 550ns<br>7mA | 3×$10^4$<br>/200 | 2016<br>/[76] |
| B :Pt/$Ta_2O_5$/Ta/Pt<br>(Vo):7nm/NS | 40<br>/0.4 kΩ | 1.84<br>/0.1V | 0.5<br>/1mA | –0.5<br>/1mA | 1.2V 45ns<br>1.3mA | –2 V 100ns<br>1mA | NS<br>/ NS | 2016<br>/[77] |
| B: Pt/$Ta_2O_5$/W/Pt<br>(Vo):7nm/NS | 550<br>/0.4 kΩ | 2.21<br>/0.1V | 0.7<br>/1mA | –0.7<br>/1mA | 1.4V 1.5mA<br>100ns | –2V 1mA<br>100ns | NS<br>/NS | 2016<br>/[ 77] |
| B: Pt/W/Ta$O_x$/Pt<br>(Vo):7nm/3bits | $10^3$<br>/0.4 kΩ | 1.7<br>/0.1V | 1.0<br>/1mA | –1<br>/1mA | NS | –1.6 V<br>1μs | $10^4$(398K)<br>/$10^6$ | 2016<br>/[78] |
| B: Pt/Ta/Ta$O_x$/Pt<br>(Vo):7nm/NS | $10^2$<br>/0.4 kΩ | 1.9<br>/0.1V | 0.75<br>/1mA | –1<br>/1mA | NS | –1.6 V<br>1μs | $10^4$(398K)<br>/$10^6$ | 2016<br>/[78] |
| B: Au/Al-ZnO/FTO<br>(Vo):300nm/NS | 100<br>/0.1 kΩ | 6.5<br>/NS | 2.7<br>/10mA | –2.5<br>/10mA | / | / | $10^3$/100 | 2016<br>/[79] |
| B: Ti/HfAl$O_x$/Pt<br>(Vo)：6.5nm/NS | 100<br>/0.75 kΩ | 3.75<br>/0.5V | 1.3<br>/1.7mA | –1.8<br>/1.7mA | / | / | 7200/$10^5$ | 2017<br>/[80] |

| | | | | | | | | |
|---|---|---|---|---|---|---|---|---|
| B: Ti/$Al_2O_3$/Pt<br>(Vo)：6.5nm/NS | 20<br>/0.7 kΩ | 3.85<br>/0.5V | 1.3<br>/5mA | －1.3<br>/3.2mA | / | / | 7200/$10^4$ | 2017<br>/[80] |
| B:Al/Mn1%:NiO/ITO<br>(Vo):120nm/NS | $10^6$<br>/0.1 kΩ | 4.5<br>/1V | 3.1<br>/1mA | –2.5<br>/1mA | / | / | $10^4$/100 | 2017<br>/ [81] |
| B: Ag/NiO/Pt<br>(Vo):50nm/NS | $10^2$<br>/0.3 kΩ | 1.25<br>/0.1V | 0.5<br>/1mA | –0.5<br>/1mA | / | / | $10^5$/100 | 2018<br>/[82] |
| B: Ti/$HfO_2$/TiN<br>(Vo):10nm/NS | 10<br>/10 kΩ | 2.9<br>/0.1V | 0.5V<br>/15μA | ～–0.4<br>/3μA | 1V 10μA<br>2μs | –1.2V<br>500μs | $10^4$(380K)<br>/$10^7$ | 2018<br>/[83] |
| B: ITO/a-$TiO_2$/Pt<br>(Vo):7.5nm/NS | 200/<br>30~40Ω | 4.15<br>/0.1V | 0.6<br>/10mA | –0.5<br>/10mA | / | / | $10^4$/100 | 2018<br>/[84] |
| B: ITO/$Zn_2TiO_4$/Pt<br>(Vo):67.69nm/2bits | ~$10^2$<br>/0.4 kΩ | ～0.65<br>/0.1V | 0.6<br>/1mA | –0.6<br>/5mA | / | / | $10^4$/>500 | 2018<br>/[85] |
| B: Ag/MnO/$Ta_2O_5$/Pt<br>(Vo):60nm/NS | $10^6$<br>/3 kΩ | NO<br>/0.2V | 0.8<br>/0.2mA | –1.1<br>/0.2mA | / | / | $10^4$/100 | 2018<br>/[86] |
| B:Pd/$HfO_x$/Au NCs/<br>$HfO_x$/TiN/NS<br>(Vo):16nm | ~$10^3$<br>/2 kΩ | 5.25/<br>0.2V | 1.2<br>/200μA | –1.05<br>/200μA | 2.2V 100ns<br>4mA | –2.2 V<br>150ns<br>4mA | >$10^4$(358K)<br>/$10^8$ | 2018<br>/[87] |
| B: Pd/$HfO_x$ /TiN<br>(Vo):16nm/NS | ~$10^3$<br>/2 kΩ | 9.8/0.2<br>V1μs | 1.8<br>/200μA | –1.55<br>/1mA | 3V 1.5μs<br>6mA | –3V 1.5μs<br>6mA | >$10^4$(358K)<br>/$10^6$ | 2018<br>/[87] |
| B:TaN/$CeO_{2-x}$/$TiO_2$/Pt<br>(Vo):15nm | 25<br>/0.4 kΩ | 1.5<br>/0.2V | 1~1.4<br>/1mA | –0.7<br>/1mA | / | / | $10^4$/$10^3$ | 2019<br>/[88] |
| B: TaN/ $CeO_{2-x}$ /Pt<br>(Vo):5nm/NS | 30<br>/0.7 kΩ | 2.5<br>/0.2V | 0.5<br>/10mA | －2<br>/60mA | / | / | 2×$10^3$<br>/300 | 2019<br>/[88] |
| B:TiN/($HfO_2$/$ZrO_2$)×2/Pt<br>(Vo):16nm/NS | 7-8<br>/100 kΩ | －8.7<br>/0.5V | －0.9<br>/0.1mA | 1.4<br>/0.1mA | 3V 0.1s<br>75μA | –3V 0.1s<br>75 μA | $10^5$<br>/100 | 2020<br>/[89] |
| B: Pt/$GA_2O_3$/ZnO/Pt<br>(Vo):10.5nm/NS | 40<br>/0.3 kΩ | 4<br>/0.1V | 2~2.5<br>/0.5mA | –0.5<br>/1mA | / | / | $10^4$/100 | 2020<br>/[90] |
| B: Pt/Ta/$TaO_x$/Pt<br>(Vo):10nm/NS | 20<br>/2 kΩ | 2.6<br>/0.1V | 0.7<br>/0.5mA | –1<br>/0.5mA | / | / | $10^5$(358K)<br>/4.5×$10^8$ | 2021<br>/[91] |
| B: Pt/Ta/$TaO_x$:Zr/Pt<br>(Vo):10nm/NS | >20<br>/2 kΩ | 1.5<br>/0.1V | 0.7<br>/0.5mA | –0.6<br>/0.5mA | / | / | $10^7$(358K)<br>/2.9×$10^{10}$ | 2021<br>/[91] |
| B: Pt/Ta/$ZrO_2$/Pt<br>(Vo):5nm/NS | >10<br>/0.2 kΩ | NS<br>/0.2V | 0.9<br>/0.34mA | –0.8<br>/0.3mA | / | / | NS<br>/8×$10^5$ | 2021<br>/[ 92] |
| B: Pt/$HfO_x$/Polydopamine<br>/Ag NPs/Ti, (Vo or weak<br>metal) :5nm/NS | 100<br>/0.2 kΩ | Yes<br>/0.1V | 0.5<br>/1mA | –0.7<br>/1mA | 0.9V<br>70ns | –1.3V<br>70ns | $10^4$(358K)<br>/$10^3$ | 2021<br>/[93] |
| B: Ti/$HfO_x$/Cu/$HfO_x$/Pt<br>(Vo+Cu):20nm/NS | ~33<br>/50Ω | 0.43<br>/0.05V | 0.16<br>/10mA | –0.14<br>/7mA | 0.17V<br>82ns | / | $10^4$/200 | 2021<br>/[94] |
| B: Ta/$Ta_2O_5$/$ZrO_2$/Pt<br>(Vo):12nm/5bits | 100<br>/0.2 kΩ | 2.6/0.2<br>V10μs | 0.99<br>/1mA | –0.64<br>/1mA | 1.5V 1mA<br>10μs | –2V 1mA<br>10μs | $10^4$/$10^5$ | 2021<br>/[95] |

| | | | | | | | | |
|---|---|---|---|---|---|---|---|---|
| B: Ta/ $ZrO_2$/Pt<br>(Vo):10nm/NS | $10^3$<br>/0.2 kΩ | 3.2<br>/0.2 | 0.82<br>/1mA | –0.67<br>/1mA | / | / | NS/100 | 2021<br>/[95] |
| B: W/$TiO_2$/$HfO_2$/TaN<br>(Vo):10nm/NS | 10<br>/3.3 kΩ | 5<br>/0.2V | 0.6<br>/100μA | –0.6<br>/100μA | 1V<br>10μs | –1V<br>10μs | $10^4$(398K)<br>/$10^7$ | 2022<br>/[96] |
| B:Au/$HfO_2$/Al-ZnO/$HfO_2$<br>/ITO, (Vo):100nm/5bits | $10^4$<br>/0.3 kΩ | 4.4<br>/0.45V | 0.65<br>/1mA | –1.34<br>/1mA | / | / | $10^4$(353K)<br>/$10^2$ | 2022<br>/[97] |
| B: ITO/$WO_x$/ITO<br>(Vo):15nm/NS | 6<br>/1 kΩ | －5/ –<br>0.2V | －1.9<br>/0.2mA | 2<br>/0.2mA | 1.5V<br>10μs | 2V<br>10μs | $10^4$/300 | 2022<br>/[98] |
| B: Pt-$Au_{min}$/$NbO_x$/W<br>(Vo):106nm/NS | 1200/<br>~0.06<br>kΩ | Yes<br>/NS | 1.3<br>/5mA | –0.59<br>/5mA | / | / | NS/350 | 2024<br>/[99] |
| B: Au/$ZrO_2$/ITO<br>(Vo):25nm/NS | 100<br>/3 kΩ | 4.8<br>/0.2V | 1.66<br>/0.5mA | –1.55<br>/0.5mA | / | / | $10^3$/500 | 2024<br>/[29] |
| B: Ag/$TiO_xN_y$/$Ga_2O_3$/Pt<br>(Ag+Vo):33.97nm/7bits | $10^6$<br>/0.2 kΩ | NO<br>/0.05V | 0.17<br>/1mA | –0.057<br>/0.2mA | / | / | $10^4$/50 | 2024<br>/[100] |

**3.Quartile and IQR analysis**

Using the data from Table 1 in the main text and Tables S1-S3 in this supplement material, We calculated the 95% confidence intervals for the 50th percentile and IQR of all parameters across the five device types, which are listed in Tables S4 and S5, respectively.

Table S4 50th Percentiles and Confidence Intervals of the Parameters

| Name | Ag CFD | | Cu CFD | | Ni CFD | | Co CFD | | VCM device | |
|---|---|---|---|---|---|---|---|---|---|---|
| | 50th | CI* | 50th | CI | 50th | CI | 50th | CI | 50th | CI |
| $R_{LRS}$ (kΩ) | 0.4 | [0.10, 0.50] | 2.15 | [1.50, 5.00] | 0.167 | [0.066, 0.8] | 6 | [0.6, 20] | 0.40 | [0.23, 0.75] |
| L(nm) | 25 | [20, 50] | 12 | [9, 20] | 20 | [6.5, 22] | 7 | [6, 30] | 20 | [13.5, 25] |
| MW | 1075 | [$10^3$, $6.34\times10^4$] | $10^3$ | [$10^2$, $10^5$] | $10^3$ | [$10^2$, $10^4$] | 550 | [$10^2$, $10^3$] | 100 | [45, 200] |
| $V_F$ (V) | 1.675 | [0.72, 2.25] | 3.50 | [2.50, 4.00] | 4.42 | [3.00, 7.20] | 3.8 | [2.30, 5.00] | 3.40 | [2.55, 4.00] |
| $V_{Set}$ (V) | 0.675 | [0.50, 0.91] | 1.00 | [0.80, 1.30] | 2.00 | [1.40, 3.00] | 1.75 | [1.35, 2.40] | 1.00 | [0.80, 1.20] |
| $\lvert V_{Reset}\rvert$ (V) | 0.485 | [0.40, 0.665] | 0.64 | [0.50, 1.00] | 0.80 | [0.60, 1.20] | 0.65 | [0.50, 1.20] | 1.00 | [0.70, 1.10] |
| $P_{Smean}$ (μW/bit) | 54.21 | [28.868, 128.30] | 17.641 | [8.660, 57.735] | 102.640 | [13.472, 1539.600] | 10.264 | [6.415, 96.225] | 54.528 | [32.075, 76.980] |
| $P_{Rmean}$ (μW/bit) | 128.94 | [67.098, 384.90] | 19.25 | [10.59, 115.47] | 1347.72 | [250.19, 1924.5] | 57.74 | [9.63, 269.43] | 180.90 | [109.70, 389.71] |
| $V_{Read}$ (V) | 0.10 | [0.10, 0.10] | 0.20 | [0.1, 0.2] | 0.10 | [0.1, 0.2] | 0.10 | [0.1, 0.2] | 0.20 | [0.1, 0.2] |
| $P_{Lread}$ (μW/bit) | 54.99 | [20, 100] | 12.5 | [4.76, 40.00] | 125 | [50.00, 500.00] | 13.0 | [0.55, 61.91] | 50.0 | [25,125] |
| $P_{Hread}$ (μW/bit) | $3.19\times10^{-2}$ | [$2.17\times10^{-3}$, , $1.47\times10^{-1}$] | $1.84\times10^{-2}$ | [$1.18\times10^{-3}$, $5.50\times10^{-2}$] | 0.113 | [$8\times10^{-3}$, 2.00] | 0.013 | [$5.5\times10^{-4}$, 1.95] | 0.25 | [0.13, 1.21] |
| $V_{Write}$ (V) | 1.500 | [1.00, 2.50] | 2.50 | [1.50, 3.50] | 3.00 | [1.40, 9.00] | 3.70 | [1.5, 6.0] | 1.70 | [1.40, 2.20] |
| $t_{Write}$ (μs) | 50.000 | [5.00, 400] | 0.175 | [0.10, 0.22] | 0.05 | [0.02, 200] | 0.1 | [0.07, 0.40] | 0.20 | [0.01, 10.00] |
| $P_{Write}$ (μW/bit) | 195.000 | [100.000, 400.000] | 132.500 | [34.500, 312.500] | $1.508\times10^3$ | [14.500, $7.125\times10^4$] | 21.000 | [18.5, 375] | 200.00 | [118.00, 780.00] |
| $\lvert V_{Erase}\rvert$ (V) | 1.95 | [1.00, 2.50] | 2.50 | [1.50, 3.00] | 2.10 | [0.60, 8.00] | 1.50 | [1.30, 1.60] | 2.00 | [1.80, 2.20] |
| $t_{Erase}$ (μs) | 50.00 | [5.00, 225] | 0.10 | [0.10, 0.31] | 0.05 | [0.03, 200] | 3.00 | [0.48, 8.00] | 0.55 | [0.14, 10] |
| $P_{Erase}$ (μW/bit) | 1000.0 | [650.0，12583.3] | 26.667 | [80, 2250] | $3.850\times10^3$ | [450,$1.68\times10^4$] | 25.833 | [19.167, $1.466\times10^3$] | 783.33 | [440,3133.30] |
| $E_{Write}$ (nJ/bit) | 3.250 | [0.017, 37.50] | $4.500\times10^{-2}$ | [$3.600\times10^{-3}$, $9.625\times10^{-2}$] | 3.000 | [$4.45\times10^{-3}$, $1.128\times10^3$] | $2.625\times10^{-2}$, | [$3.800\times10^{-3}$, 0.168] | $4.950\times10^{-2}$ | [$8.800\times10^{-3}$ 135.75] |

| | | | | | | | | | | |
|---|---|---|---|---|---|---|---|---|---|---|
| $E_{Erase}$ (nJ/bit) | 19.167 | [0.213, 83.333] | $1.000 \times 10^{-1}$ | [$8.000\times 10^{-3}$, $9.000\times 10^{-1}$] | 17.518 | [$2.85\times10^{-2}$, $2.684\times10^{3}$] | $2.600 \times10^{-1}$ | [$2.125\times10^{-2}$, $9.973\times10^{-1}$] | 0.340 | [$8.13\times10^{-2}$, 451.28] |
| Endurance (cycles) | 650 | [200, $10^4$] | $10^4$ | [800, $10^5$] | 150 | [80, $10^3$] | $10^3$ | [$10^2$, $10^5$] | 500 | [150, $10^5$] |
| Retention (s) | $2\times10^4$ | [$10^4$, $5\times10^4$] | $10^4$ | [$10^{4,}$ $10^5$] | $3.5\times10^4$ | [$10^4$, $10^5$] | $3.6\times 10^3$ | [$3.6\times10^3$, $10^5$] | $10^4$ | [$10^4$, $10^5$] |
| L(nm) | 25 | [20, 47] | 12 | [9, 20] | 20 | [6.5, 22] | 7 | [6, 30] | 20 | [13.5, 25] |
| Multilevel (bits/cell) | 5 | [3,6] | 4 | [3, 6] | / | / | / | / | 4 | [3, 5] |

*CI denotes the confidence interval, where the confidence level is 95%.

Table S5. Calculation Results of Quartiles and IQR of Devices

| Type | Ag filament devices | | | | Cu filament devices | | | | Ni filament devices | | | | Co filament devices | | | | VCM devices | | | |
|---|---|---|---|---|---|---|---|---|---|---|---|---|---|---|---|---|---|---|---|---|
| | $Q_1$ | $Q_2$ | $Q_3$ | IQR | $Q_1$ | $Q_2$ | $Q_3$ | IQR | $Q_1$ | $Q_2$ | $Q_3$ | IQR | $Q_1$ | $Q_2$ | $Q_3$ | IQR | $Q_1$ | $Q_2$ | $Q_3$ | IQR |
| $R_{LRS}$(kΩ) | 0.100 | 0.400 | 1.000 | 0.900 | 1.00 | 2.150 | 10.0 | 9.00 | 0.054 | 0.167 | 0.875 | 0.821 | 0.550 | 6.000 | 20.000 | 19.45 | 0.120 | 0.400 | 2.000 | 1.880 |
| L(nm) | 20 | 25 | 58 | 38 | 7 | 12 | 30 | 23 | 5 | 20 | 28 | 23 | 5 | 7 | 30 | 25 | 10 | 20 | 40 | 30 |
| Multiplevel (bits/cell) | 4 | 5 | 5 | 1 | 3 | 4 | 5 | 2 | / | / | / | / | / | / | / | / | 3 | 4 | 5 | 2 |
| MW | $1.270 \times10^2$ | $1.075 \times10^3$ | $10^6$ | $\sim10^6$ | $1.00 \times10^2$ | $10^3$ | $10^4$ | $9.9 \times10^3$ | $10^2$ | $10^3$ | $10^4$ | 9900 | $10^2$ | $5.50 \times10^2$ | $10^3$ | 900 | $2.50 \times10^1$ | $10^2$ | $10^3$ | 9750 |
| $V_F$(V) | 0.600 | 1.675 | 2.500 | 1.900 | 2.20 | 3.500 | 4.715 | 2.515 | 3.00 | 4.420 | 7.125 | 4.125 | 2.350 | 3.800 | 5.000 | 2.650 | 1.840 | 3.400 | 4.500 | 2.660 |
| $V_{Set}$(V) | 0.240 | 0.675 | 1.00 | 0.760 | 0.683 | 1.000 | 2.00 | 1.318 | 1.175 | 2.000 | 3.000 | 1.825 | 1.350 | 1.750 | 2.400 | 1.050 | 0.700 | 1.000 | 1.700 | 1.000 |
| $V_{Reset}$(V) | 0.150 | 0.485 | 0.800 | 0.650 | 0.50 | 0.640 | 1.125 | 0.625 | 0.600 | 0.800 | 1.275 | 0.675 | 0.500 | 0.650 | 1.200 | 0.700 | 0.600 | 1.000 | 1.500 | 0.900 |
| $P_{Smean}$ (μW/bit) | 7.057 | 54.210 | $2.053 \times10^2$ | $1.982 \times10^2$ | 5.292 | $1.764 \times10^1$ | $8.275 \times10^1$ | $7.746 \times10^1$ | $1.251 \times10^1$ | $1.026 \times10^2$ | $1.796 \times10^3$ | $1.784 \times10^3$ | 6.816 | $1.026 \times10^1$ | $8.340 \times10^1$ | $7.658 \times10^1$ | $2.245 \times10^1$ | $5.453 \times10^1$ | $2.245 \times10^2$ | $2.021 \times10^2$ |
| $P_{Rmean}$ (μW/bit) | 9.045 | $1.2894\times 10^2$ | $4.619\times 10^2$ | 4.528 $10^2$ | 9.442 | $1.925 \times10^1$ | $2.309 \times10^2$ | $2.215 \times10^2$ | $2.261 \times10^2$ | $1.347 \times10^3$ | $2.021 \times10^3$ | $1.795 \times10^3$ | $1.023 \times10^1$ | $5.774 \times10^1$ | $2.261 \times10^2$ | $2.141 \times10^2$ | $5.774 \times10^1$ | $1.809 \times10^2$ | $8.006 \times10^2$ | $7.429 \times10^2$ |
| $V_{Read}$(V) | 0.100 | 0.100 | 0.100 | 0 | 0.10 | 0.20 | 0.30 | 0.2 | 0.10 | 0.10 | 0.275 | 0.175 | 0.100 | 0.100 | 0.200 | 0.100 | 0.100 | 0.200 | 0.300 | 0.200 |
| $P_{ReadLRS}$ (μW/bit) | $1\times 10^1$ | $5.499\times 10^1$ | $1.00\times 10^2$ | 90.0 | $0.350 \times10^1$ | $1.250 \times10^1$ | $4.865 \times10^1$ | $4.515 \times10^1$ | $4.861 \times10^1$ | $1.250 \times10^2$ | $5.139 \times10^2$ | $4.653 \times10^2$ | 1.000 | $1.300\times 10^1$ | $5.714\times 10^1$ | $5.614\times 10^1$ | $2.125 \times10^1$ | $5.000 \times10^1$ | $2.770 \times10^2$ | $2.556 \times0^2$ |

| $P_{ReadHRS}$ (μW/bit) | $10^{-4}$ | $0.319\times10^{-1}$ | $2.500\times10^{-1}$ | ~0.25 | $3.000\times10^{-4}$ | $0.184\times10^{-1}$ | $5.000\times10^{-1}$ | ~0.5 | $6.000\times10^{-3}$ | $1.125\times10^{-1}$ | 2.250 | 2.244 | $10^{-3}$ | $0.13\times10^{-1}$ | $5.714\times10^{-1}$ | $5.704\times10^{-1}$ | $0.341\times10^{-1}$ | 0.250 | 2.000 | 1.967 |
|---|---|---|---|---|---|---|---|---|---|---|---|---|---|---|---|---|---|---|---|---|
| $V_{Write}$(V) | 1.0 | 1.500 | 2.63 | 1.63 | 1.300 | 2.500 | 4.000 | 2.700 | 1.475 | 3.0 | 5.100 | 3.625 | 3.000 | 3.700 | 4.650 | 1.650 | 1.300 | 1.700 | 2.750 | 1.450 |
| $t_{Write}$(μs) | 3.78 | 50.000 | 425 | 421.23 | 0.100 | 0.175 | 1.000 | 0.9000 | 0.040 | 0.050 | 51.50 | 51.460 | 0.0925 | 0.100 | 0.250 | 0.158 | 0.100 | 0.200 | 10.000 | 9.900 |
| $P_{Write}$ (μW/bit) | $1.000\times10^{2}$ | $1.950\times10^{2}$ | $4.000\times10^{2}$ | $3.000\times10^{2}$ | $3.300\times10^{1}$ | $1.325\times10^{2}$ | $3.750\times10^{2}$ | $3.420\times10^{2}$ | $3.000\times10^{3}$ | $7.125\times10^{3}$ | $1.125\times10^{4}$ | $8.250\times10^{3}$ | $1.863\times10^{1}$ | $2.100\times10^{1}$ | $3.750\times10^{2}$ | $3.564\times10^{2}$ | $8.000\times10^{1}$ | $2.000\times10^{2}$ | $8.800\times10^{2}$ | $8.000\times10^{2}$ |
| $V_{Erase}$(V) | 1.00 | 1.950 | 2.75 | 1.75 | 1.275 | 2.500 | 3.000 | 1.725 | 1.65 | 2.10 | 4.10 | 2.45 | 1.350 | 1.500 | 1.600 | 0.250 | 1.600 | 2.000 | 2.375 | 0.775 |
| $t_{Erase}$(μs) | 2.65 | 50.00 | 250 | 248.4 | 0.100 | 0.100 | 0.705 | 0.605 | 0.05 | 0.05 | 53.75 | 53.71 | 0.590 | 3.000 | 7.250 | 6.660 | 0.100 | 0.550 | 57.500 | 57.400 |
| $P_{Erase}$ (μW/bit) | $6.50\times10^{2}$ | $1.000\times10^{3}$ | $1.583\times10^{3}$ | $9.333\times10^{2}$ | $7.750\times10^{1}$ | $2.667\times10^{2}$ | $2.771\times10^{3}$ | $2.693\times10^{3}$ | $7.000\times10^{3}$ | $1.683\times10^{4}$ | $1.79\times10^{4}$ | $2.667\times10^{4}$ | $2.500\times10^{1}$ | $2.583\times10^{1}$ | $1.333\times10^{3}$ | $1.308\times10^{3}$ | $2.130\times10^{2}$ | $7.833\times10^{2}$ | $3.333\times10^{3}$ | $3.120\times10^{3}$ |
| $E_{Write}$ (nJ/bit) | $1.700\times10^{-2}$ | 3.250 | $3.750\times10^{1}$ | $3.748\times10^{1}$ | $3.300\times10^{-3}$ | $4.500\times10^{-2}$ | $1.100\times10^{-1}$ | $1.067\times10^{-1}$ | 6.000 | $1.128\times10^{3}$ | $2.250\times10^{3}$ | $2.244\times10^{3}$ | $4.700\times10^{-3}$ | $2.625\times10^{-2}$ | $1.382\times10^{-1}$ | $1.335\times10^{-1}$ | $8.000\times10^{-3}$ | $4.950\times10^{-2}$ | $2.700\times10^{2}$ | $2.700\times10^{2}$ |
| $E_{Erase}$ (nJ/bit) | $2.125\times10^{-1}$ | $1.917\times10^{1}$ | $8.333\times10^{1}$ | $8.312\times10^{1}$ | $7.750\times10^{-3}$ | $1.000\times10^{-1}$ | $9.083\times10^{-1}$ | $9.006\times10^{-1}$ | $3.500\times10^{1}$ | $2.684\times10^{2}$ | $3.556\times10^{2}$ | $3.555\times10^{2}$ | $4.000\times10^{-2}$ | $2.600\times10^{-1}$ | $7.680\times10^{-1}$ | $7.280\times10^{-1}$ | $6.667\times10^{-2}$ | $3.400\times10^{-1}$ | $9.000\times10^{2}$ | $9.000\times10^{2}$ |
| Endurance (cycles) | 100 | 650 | $10^{4}$ | $9.900\times10^{3}$ | 236 | $10^{4}$ | $10^{6}$ | $\sim10^{6}$ | 60 | 150 | $10^{3}$ | 940 | 100 | $10^{3}$ | $10^{5}$ | $\sim10^{5}$ | 100 | 500 | $10^{6}$ | $\sim10^{6}$ |
| Retention (s) | $10^{4}$ | $2\times10^{4}$ | $10^{5}$ | $9.0\times10^{4}$ | $10^{4}$ | $10^{4}$ | $10^{5}$ | $9.0\times10^{4}$ | $10^{4}$ | $3.5\times10^{4}$ | $10^{5}$ | $9.000\times10^{4}$ | $3.600\times10^{3}$ | $3.600\times10^{3}$ | $5.180\times10^{4}$ | $4.820\times10^{4}$ | $10^{4}$ | $10^{4}$ | $10^{4}$ | 0 |

## 4. Non-parametric statistic method

The concepts of quantiles and the IQR are illustrated in Fig. 1. The 50th quantile represents the central value of the dataset, meaning 50% of the data points lie below it and 50% lie above it. A key property of the 50th percentile is that it is a robust measure of central tendency, as it is less influenced by extreme outliers than the mean. The IQR, which measures the spread of the middle 50% of the data, is similarly robust.

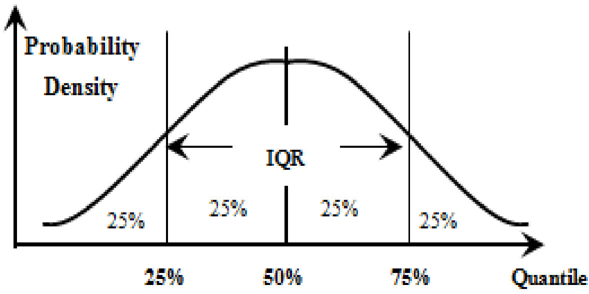


Fig. 1. Schematic diagram of the relationship between quantiles, IQR, and a symmetric probability density distribution.

In this study, the confidence level of the 50th percentile is set to 0.95, and the confidence level calculation formula is:

$$P\{y_1 < u_{50\%} < y_N\} = \sum_{i=1}^{N-1} \binom{N}{i} (0.5)^N = 0.95$$

Solving the above equation, we obtain N = 6. This implies that for a 95% confidence level, a dataset must contain at least 6 samples. In this study, the sample sizes for all five device types satisfy this requirement.

The aforementioned analysis method was implemented as a program and executed in MATLAB R2016a.

The conclusions drawn from non-parametric statistics are distribution-free, meaning they do not rely on assumptions about the underlying data distribution. This property makes them more robust compared to those derived from parametric statistical inference.

## 5. Calculation of parameters for flash devices

This section calculates the parameters of several flash memory devices that are used in the main text, including the read power consumption of both NOR and NAND flash, the erase energy of NAND flash, and the output resistance of NOR and NAND flash devices.

### 5.1. Read power consumption

The data for the NAND flash is sourced from the Micron MT29F4G08ABADAWP (4Gb SLC Parallel NAND Flash) [101]. During read operations, the chip operates with an applied voltage $V_{CC}$ = 3.3V and a sequential read current $I_{CC1}$ = 25mA. The read power ($P_{total}$) is calculated as follows:

$$P_{total} = V_{CC} \times I_{CC1} = 0.0825\text{W}$$

The read cycle time is 20 ns, and the clock frequency ($f_{CLK}$) is given by $f_{CLK}$ = 1 / (read cycle time). This is an 8-bit interface, so the data rate ($d_{rate}$) is calculated as

$$d_{rate} = f_{CLK} \times 8 = 4 \times 10^8\text{bit/s}$$

The power consumption per bit ($P_{bit}$) is

$$P_{bit} = \frac{P_{total}}{d_{rate}} = 0.2063\text{nW/bit} \qquad (2)$$

The data for the NOR flash device is sourced from the Winbond W25Q128JV (SPI NOR Flash) [102]. The operating voltage ranges from 2.7 V to 3.6 V, with an average value taken as $V_{CC}$= 3.3 V. The read operating current ($I_{CC3}$) refers to the value in Quad SPI mode. At $f_{CLK}$= 104 MHz, $I_{CC3}$ is equal to 20 mA. The read power is calculated as:

$$P_{total} = V_{CC} \times I_{CC3} = 0.066\text{W}$$

In Quad SPI mode, since four data lines are used simultaneously, four bits are transmitted per clock cycle. The data rate is calculated as

$$d_{rate} = f_{CLK} \times 4 = 4.16 \times 10^8\text{bit/s}$$

The power consumption per bit is

$$P_{bit} = \frac{P_{total}}{d_{rate}} = 0.1587\text{nW/bit}$$

### 5.2. Erase energy of NAND flash

The erase energy parameters for the NAND flash are sourced from reference [103]. The chip is erased on a block-by-block basis, with a block capacity of 8 MB. The

erase voltage $V_{CC}$=18V, the erase current $I_{CC}$=150$\mu$A, and the erase time $t_{Er}$= 3.2 ms. The total energy required to erase one block is calculated as

$$\mathrm{E}_{total} = V_{CC} \times I_{CC} \times t_{Er} = 8.64 \times 10^{-6}\mathrm{J}$$

Given that 8 MB = 8 × 1024 × 1024 bytes × 8 bits = 6.71 × $10^7$bits, the erase energy per bit is

$$E_{Erase} = \frac{E_{total}}{6.71 \times 10^7} = 1.2876 \times 10^{-4}\mathrm{nJ/bit}$$

### 5.3. Output resistance of NOR and NAND flash

The output resistance data for NAND Flash is obtained from reference [104]. The wordline (gate, $V_g$) voltage is 4.5 V, the bitline precharge voltage (drain voltage) is 1 V, and the source voltage ($V_S$) is 0 V, resulting in $V_{DS}$= 1 V. The I-V curve in Fig. 4 of the paper shows that at Vgs= 4.5 V and $V_{DS}$= 1.0 V, the current $I_{CC}$ is approximately 35 μA. Thus, the LRS value is

$$R_{LRS} = \frac{V_{DS}}{I_{cell}} = 28.57\mathrm{k\Omega}$$

In the programmed state, the cell exhibits a HRS. The paper mentions that the cell current in this state is an extremely low leakage current, near the off state. We assume that the drain-source voltage in the cutoff state is 10 V and the cutoff current is 1 μA. The resistance in the HLS can then be calculated as

$$R_{HLS} = \frac{10V}{1\mu A} = 10\mathrm{M\Omega}$$

The memory window is calculated as

$$\mathrm{MW} = \frac{R_{HRS}}{R_{LRS}} \geq 348 \approx 350$$

The output resistance data for the NOR Flash is sourced from reference [105]. With a wordline (gate) voltage of 10 V, a bitline voltage ($V_D$) of 5.0 V, and a source voltage ($V_S$) of 0 V, the write cell current ($I_{cell}$) ≥ 300 μA. During writing, the output resistance in the LRS is calculated as

$$R_{LRS} \leq \frac{V_{DS}}{I_{cell}} = 16.667\mathrm{k\Omega}$$

In the erased state, the current is extremely small, indicating that the resistance in the HRS is very high. We also assume a resistance of $R_{HRS}$= 10 MΩ in this case. This results in a memory window of

$$\mathrm{MW} \geq \frac{R_{HRS}}{R_{LRS}} = 600$$

## 6. Conclusions

This article presents experimental data for devices based on Ag, Ni, and Co conductive filaments, as well as for VCM devices. The quartiles and the IQR for these four device types, as well as for the previously discussed Cu conductive filament devices, are calculated. A brief introduction to non-parametric statistical methods is also provided. Finally, a set of parametric values for flash memory devices is calculated to enable a direct comparison with the resistive switching technologies presented in the main text.

## References

[1] Schindler C, Meier M, Waser R, et al. Resistive switching in Ag-Ge-Se with extremely low write currents[C]//2007 Non-Volatile Memory Technology Symposium. IEEE, 2007: 82-85.

[2] Yang Y C, Pan F, Liu Q, et al. Fully room-temperature-fabricated nonvolatile resistive memory for ultrafast and high-density memory application[J]. Nano letters, 2009, 9(4): 1636-1643.

[3] Symanczyk R, Bruchhaus R, Kund M. Investigation of the reliability behavior of conductive-bridging memory cells[J]. IEEE electron device letters, 2009, 30(8): 876-878.

[4] Gao S, Chen C, Zhai Z, et al. Resistive switching and conductance quantization in Ag/SiO2/indium tin oxide resistive memories[J]. Applied Physics Letters, 2014, 105(6).

[5] Devulder W, Opsomer K, Meersschaut J, et al. Combinatorial study of Ag–Te thin films and their application as cation supply layer in CBRAM cells[J]. ACS combinatorial science, 2015, 17(5): 334-340.

[6]Kwon K C, Song M J, Kwon K H, et al. Nanoscale CuO solid-electrolyte-based conductive- bridging

-random-access-memory cell operating multi-level-cell and 1selector1resistor[J]. Journal of Materials Chemistry C, 2015, 3(37): 9540-9550.

[7] Huang Y, Shen Z, Wu Y, et al. Amorphous ZnO based resistive random access memory. RSC adv, 2016, 6（22）: 17867-17872

[8] Zhou G, Xiao L, Zhang S, et al. Mechanism for an enhanced resistive switching effect of bilayer $NiO_x/TiO_2$ for resistive random access memory. J. Alloys and Compounds, 2017, 722: 753-759

[9] Tseng Y T, Chen I, Chang T C, et al. Enhanced electrical behavior from the galvanic effect in Ag-Cu alloy electrode conductive bridging resistive switching memory[J]. Applied Physics Letters, 2018, 113(5).

[10] Yan X, Qin C, Lu C, et al. Robust $Ag/ZrO_2/WS_2/Pt$ memristor for neuromorphic computing[J]. ACS applied materials & interfaces, 2019, 11(51): 48029-48038.

[11] Kuo C C, Chen I C, Shih C C, et al. Galvanic effect of Au–Ag electrodes for conductive bridging resistive switching memory[J]. IEEE Electron Device Letters, 2015, 36(12): 1321-1324.

[12] Li Y, Yin L, Wu Z, et al. Improved resistive switching uniformity of $SiO_2$ electrolyte-based resistive random access memory device with Cu oxidizable electrode[J]. IEEE Electron Device Letters, 2019, 40(10): 1599-1601.

[13] Rebora C, Huang R, Kissling G P, et al. Conductive-bridge memory cells based on a nanoporous electrodeposited GeSbTe alloy[J]. Nanotechnology, 2019, 30(2): 025202.

[14] Jeon Y R, Abbas Y, Sokolov A S, et al. Study of in situ silver migration in amorphous boron nitride CBRAM device[J]. ACS applied materials & interfaces, 2019, 11(26): 23329-23336.

[15] Wang Z Q, Xu H Y, Li X H, et al. Synaptic learning and memory functions achieved using oxygen ion migration/diffusion in an amorphous InGaZnO memristor. Adv. Funct. Mater., 2012, 22（13）: 2759-276

[16] Kumari A, Shanbogh S M, Udachyan I, et al. Interface-driven multifunctionality in two-dimensional $TiO_2$ nanosheet/poly（dimercaptothiadiazole-triazine）hybrid resistive random access
memory device. ACS Appl. Mater. Interfaces, 2020, 12（50）: 56568-56578

[17] Ali A, Abbas Y, Abbas H, et al. Dependence of InGaZnO and SnO2 thin film stacking sequence for the resistive switching characteristics of conductive bridge memory devices[J]. Applied Surface Science, 2020, 525: 146390.

[18]Senapati A, Roy S, Lin Y F, et al. Oxide-electrolyte thickness dependence diode-like threshold switching and high on/off ratio characteristics by using Al2O3 based CBRAM[J]. Electronics, 2020, 9(7): 1106.

[19]Lian, Xiaojuan; Shen, Xinyi; Fu, Jinke; Gao, Zhixuan; Wan, Xiang; Liu, Xiaoyan; Hu, Ertao; Xu, Jianguang; Tong, Yi . (2020) Electrical Properties and Biological Synaptic Simulation of $Ag/MXene/SiO_2/Pt$ RRAM Devices. Electronics, 9(12): 2098. doi:10.3390/electronics9122098

[20] Wang T Y, Meng J L, Li Q X, et al. Forming-free flexible memristor with multilevel storage for neuromorphic computing by full PVD technique. J Mater Sci Technol, 2021, 60: 21-26

[21] Banerjee W, Kim S H, Lee S, et al. An efficient approach based on tuned nanoionics to maximize memory characteristics in Ag - based devices[J]. Advanced Electronic Materials, 2021, 7(4): 2100022.

[22] Ali, A.; Abbas, H., Hussain, M., Jaffery, S.H.A., Hussain, S.,Choi, C.,Jung, J. Thickness-Dependent Monochalcogenide GeSe-Based CBRAM for Memory and Artificial Electronic Synapses. Nano Res. 2022, 15, 2263–2277.

[23] Hsu C C, Hua S Y, Zhang X Z, et al. Effects of interfacial oxide layer formed by annealing process on WORM characteristics of $Ag/Cu_xO/SiO_x/n^+$–Si devices. J. Alloys and Compounds, 2022, 898: 162918

[24] Ali A, Abbas H, Li J, et al. GeS conducting-bridge resistive memory device with IGZO buffer layer for highly uniform and repeatable switching[J]. Applied Physics Letters, 2023, 122(20).

[25] Mohanty S K, Panda D, Wu C H, et al. Controlling diffusion dynamics with electrode engineering for stable and reliable resistive switching in AlN/Ag-based CBRAM[J]. Materials Today: Proceedings, 2023.

[26] Han S W, Shin M W. $Al_2O_3$ interfacial layer derived hybrid conductive filament for the reliability enhancement of $Ta_2O_5$-based resistive random access memory[J]. Journal of Alloys and Compounds, 2023, 960: 170902.

[27] Jiyeon Ryu, Kitae Park, Dwipak Prasad Sahu, and Tae-Sik Yoon. Forming-Free, Low-Voltage, and High-Speed Resistive Switching in Ag/Oxygen-Deficient Vanadium Oxide(VOx)/Pt Device through Two-Step Resistance Change by Ag Filament Formation. ACS Appl. Mater. Interfaces 2024, 16, 26450−26459

[28] C. Tsioustas,a) P. Bousoulas, G. Kleitsiotis, S. D. Mantas, and D. Tsoukalas. Impact of inert electrode on the volatility and non-volatility switching behavior of $SiO_2$-based conductive bridge random access memory devices. Appl. Phys. Lett. 125, 023508 (2024); doi: 10.1063/5.0209676

[29] Aziz J, Khan M F, Neumaier D, et al. Controlled Charge Transport in ZrO2 and its Bilayer Structures for Low-Power Memory[J]. Journal of Alloys and Compounds, 2024: 175103.

[30] Sun T, Yu F, Li C, et al. Stable and repeatable $ZrO_2$ RRAM achieved by NiO barrier layer for negative set phenomenon elimination[J]. Solid-State Electronics, 2024, 217: 108948.

[31] Tran X A, Yu H Y, Gao B, et al. Ni Electrode Unipolar Resistive RAM Performance Enhancement by $AlO_y$ Incorporation Into $HfO_x$ Switching Dielectrics [J]. IEEE electron device letters, 2011, 32(9): 1290-1292.

[32] X. A. Tran, H. Y. Yu, Y. C. Yeo, L. Wu, W. J. Liu, Z. R. Wang, Z. Fang, K. L. Pey, X. W. Sun, A. Y. Du, B. Y. Nguyen, and M. F. Li. A High-Yield HfOx-Based Unipolar Resistive RAM Employing Ni Electrode Compatible With Si-Diode Selector for Crossbar Integration. IEEE Electron Device Letters, 2011, 32(3): 396-398.

[33] Tran X A, Gao B, Kang J F, et al. High performance unipolar $AlO_y/HfO_x$/Ni based RRAM compatible with Si diodes for 3D application[C]//2011 Symposium on VLSI Technology-Digest of Technical Papers. IEEE, 2011: 44-45.

[34] Park J, Jeon H, Kim H, et al. Spatially confined electric field effect for improved resistive switching behavior of a Ni/Ta-embedded TaO x/NiSi device[J]. RSC Advances, 2014, 4(105): 61064-61067.

[35] Zhang X. Resistive switching characteristics of Ni/HfO2/Pt ReRAM[J]. Journal of Semiconductors, 2012, 33(5): 054011.

[36] X. A. Tran, W. Zhu, W. J. Liu, Y. C. Yeo, B. Y. Nguyen, and H. Y. Yu. Self-Selection Unipolar $HfO_x$-Based RRAM. IEEE Trans. on eletronic devices, VOL. 60, NO. 1, 2013.

[37] Jun Sun, Qi Liu, Hongwei Xie, Xing Wu, Feng Xu, Tao Xu, Shibing Long, Hangbing Lv, Yingtao Li, Litao Sun, and Ming Liu. In situ observation of nickel as an oxidizable electrode material for the solid-electrolyte-based resistive random access memory. Appl. Phys. Lett. 102, 053502 (2013); doi: 10.1063/1.4790837

[38] W H Xue, W Xiao, J Shang, X X Chen, X J Zhu, L Pan,H W Tan, W B Zhang, Z H Ji, G Liu, X-H Xu, J Ding and R-W Li. Intrinsic and interfacial effect of electrode metals on the resistive switching behaviorof zinc oxide films. Nanotechnology 25 (2014) 425204

[39]Gonzalez M B, Rafí J M, Beldarrain O, et al. Analysis of the Switching Variability in Ni/$HfO_2$-Based RRAM Devices[J]. IEEE Transactions on Device and Materials Reliability, 2014, 14(2): 769-771.

[40] Park J, Jeon H, Kim H, et al. Stabilization of Ni conductive filaments using NH 3 plasma treatment for electrochemical metallization memory[J]. RSC Advances, 2015, 5(84): 68900-68905.

[41] J-H. Ryu, F. Hussain, C. Mahata, M. Ismail, Y. Abbas, M-H. Kim, C. Choi, B-G. Park, S. Kim, Filamentary and interface switching of CMOS-compatible $Ta_2O_5$ memristor for non-volatile memory and synaptic devices,

Applied Surface Science (2020), doi: https://doi.org/10.1016/j.apsusc.2020.147167
[42]Otsuka S, Hamada Y, Ito D, et al. Magnetoresistance of conductive filament in Ni/HfO2/Pt resistive switching memory[J]. Japanese Journal of Applied Physics, 2015, 54(5S): 05ED02.
[43] Otsuka S, Hamada Y, Shimizu T, et al. Ferromagnetic nano-conductive filament formed in Ni/TiO 2/Pt resistive-switching memory[J]. Applied Physics A, 2015, 118: 613-619.
[44] Daisuke Ito, Yoshihumi Hamada, Shintaro Otsuka, Tomohiro Shimizu, and Shoso Shingubara. Oxide thickness dependence of resistive switching characteristics for Ni/HfOx/Pt resistive random access memory device. Japanese Journal of Applied Physics 54, 06FH11 (2015)
[45] Liu D, Yin Y, Cheng H. Physically transient memristor based on the permeation of water at the interface of electrode and substrate. J. Alloys and Compounds, 2019, 810: 151957
[46] Mehr Khalid Rahmani, Byung-Do Yang, HyungWon Kim1, Hyojin Kim, and Moon Hee Kang. Coexistence of volatile and non-volatile resistive switching in Ni/SiO2/Pt memristor device controlled from different current compliances. Semicond. Sci. Technol. 36 (2021) 095031
[47] Guokun Ma, Xiaoli Tang, Hua Su, Huaiwu Zhang, Jie Li, Zhiyong Zhong. Effects of electrode materials on bipolar and unipolar switching in NiO resistive switching device. Microelectronic Engineering 129 (2014) 17–20
[48] Shukla N, Ghosh R K, Grisafe B, et al. Fundamental mechanism behind volatile and non-volatile switching in metallic conducting bridge RAM[C]//2017 IEEE International Electron Devices Meeting (IEDM). IEEE, 2017: 4.3. 1-4.3. 4.
[49] Li L, Liu Y, Teng J, et al. Anisotropic magnetoresistance of nano-conductive filament in Co/HfO 2/Pt resistive switching memory[J]. Nanoscale Research Letters, 2017, 12: 1-6.
[50] Belmonte A, Radhakrishnan J, Goux L, et al. Co active electrode enhances CBRAM performance and scaling potential[C]//2019 IEEE International Electron Devices Meeting (IEDM). IEEE, 2019: 35.8. 1-35.8. 4.
[51] Radhakrishnan J, Belmonte A, Nyns L, et al. Impact of La–OH bonds on the retention of Co/LaSiO CBRAM[J]. Applied Physics Letters, 2020, 117(15).
[52] Lee C X X, Dananjaya P A, Chee M Y, et al. Enhanced resistive switching characteristics of conductive bridging memory device by a Co–Cu alloy electrode[J]. Applied Physics Letters, 2023, 123(13).
[53] Choi Y J, Bang S, Kim T H, et al. Electric-field-induced metal filament formation in cobalt-based CBRAM observed by TEM[J]. ACS Applied Electronic Materials, 2023, 5(3): 1834-1843.
[54] Cho Y, Kang B S, Kumbhare P, et al. Switching layer optimization in Co-based CBRAM for> 105 memory window in sub-100 μA regime[J]. Solid-State Electronics, 2024: 108964.
[55] Chang W, Y, Lai Y C, Wu T B, et al. Unipolar resistive switching characteristics of ZnO thin films for nonvolatile memory applications. Appl. Phys. Lett., 2008, 92（2）:022110
[56]Kim S, Choi Y K. Resistive switching of aluminum oxide for flexible memory. Appl. Phys. Lett., 2008, 92（22）: 223508
[57] Xu N, Liu L, Sun X, et al. Characteristics and mechanism of conduction/set process in TiN⁄ ZnO⁄ Pt resistance switching random-access memories. Appl. Phys. Lett., 2008, 92（23）: 232112
[58] Yang M K, Park J W, Ko T K., et al. Bipolar resistive switching behavior in Ti/$MnO_2$/Pt structure for nonvolatile memory devices. Appl. Phys. Lett., 2009, 95（4）:5655
[59]Yang J J, Zhang M X , Strachan J P, et al. High switching endurance in $TaO_x$ memristive devices. Appl. Phys. Lett., 2010, 97（23）: 232102
[60] Han Y, Cho K, Kim S. Characteristics of multilevel bipolar resistive switching in Au/ZnO/ITO devices on glass. Microelectronic Eng, 2011, 88（8）: 2608-2610
[61] Chiu F C, Li P W, Chang W Y. Reliability characteristics and conduction mechanisms in resistive

switching memory devices using ZnO thin films. Nanoscale Res Lett, 2012, 7: 1-9

[62] Hsu C W, Wang I T, Lo C L, et al. Self-rectifying bipolar $TaO_x/TiO_2$ RRAM with superior endurance over $10^{12}$ cycles for 3D high-density storage-class memory. In the IEEE Solid-State Circuits Society and the Japan Society of Applied Physics, eds. 2013 Symposium on VLSI Technology. New York: IEEE, 2013: T166-T167

[63] W. J. Liu, X. A. Tran, H. Y. Yu, and X. W. Sunb. A Self-Rectifying Unipolar HfOx Based RRAM Using Doped Germanium Bottom Electrode. ECS solid state letters, 2(5), Q35-Q38.

[64]C. Chen, S. Gao, F. Zeng, G. S. Tang, S. Z. Li, C. Song, H. D. Fu, and F. Pan. Migration of interfacial oxygen ions modulated resistive switching in oxide-based memory devices. Journal of Applied Physics 114, 014502 (2013); doi: 10.1063/1.4812486

[65] Zhao L, Chen H Y, Wu S C. Multi-level control of conductive nano-filament evolution in $HfO_2$ ReRAM by pulse-train operations. Nanoscale, 2014, 6（11）: 5698-5702

[66] Bai Y, Wu H, Wu R, et al. Study of multi-level characteristics for 3D vertical resistive switching memory. Sci Rep, 2014, 4（1）: 5780

[67] Cho K, Park S, Chung I, et al. Effect of oxidizable electrode material on resistive switching characteristics of $ZnO_xS_{1-x}$ Films. J. Nanosci. Nanotechnol., 2014, 14（11）: 8187-8190

[68] Prakash A, Park J, Song J, et al. Demonstration of low power 3-bit multilevel cell characteristics in a TaO x-based RRAM by stack engineering. IEEE Elec. Device Lett., 2014, 36 (1): 32-34

[69] Chand U, Huang C Y, Jieng J H, et al. Suppression of endurance degradation by utilizing oxygen plasma treatment in $HfO_2$ resistive switching memory. Appl. Phys. Lett., 2015, 106 (15):133441

[70] Park M R., Abbas Y, Hu Q, et al. Resistive switching characteristics of tantalum oxide thin film and titanium oxide nanoparticles hybrid structure. J. Nanosci. Nanotechnol., 2015, 15（11）: 8613-8616

[71] Won-Ho Lee, Eom-Ji Kim, and Sung-Min Yoon. Effect of Al incorporation amount upon the resistive-switching characteristics for nonvolatile memory devices using Al-doped ZnO semiconductors [J]. Journal of Vacuum Science & Technology B 33, 051216 (2015); doi: 10.1116/1.4930896

[72] Huang Y J, Shen T H, Lee L H, et al. Low-power resistive random access memory by confining the formation of conducting filaments. AIP Adv, 2016, 6（6）:809.

[73] Lu W, Chen W, Li Y, et al. Self current limiting MgO ReRAM devices for low-power non-volatile memory applications. IEEE Journal on Emerging and Selected Topics in Circuits and Systems, 2016, 6（2）: 163-170

[74] Bousoulas P, Stathopoulos S, Tsialoukis D, et al. Low-power and highly uniform 3-b multilevel switching in forming free $TiO_{2-x}$-based RRAM with embedded Pt nanocrystals. IEEE Elec. Device Lett., 2016, 37（7）: 874-877

[75] Yu M, Cai Y, Wang Z, et al. Novel vertical 3D structure of TaOx-based RRAM with self-localized switching region by sidewall electrode oxidation. Sci Rep, 2016, 6（1）: 21020

[76] Kim J, Inamdar A. I, Jo Y, et al. Effect of electronegativity on bipolar resistive switching in a $WO_3$-based asymmetric capacitor structure. ACS Appl. Mater. Interfaces, 2016, 8（14）: 9499-9505

[77] Kim W, Menzel S, Wouters D J, et al. Impact of oxygen exchange reaction at the ohmic interface in $Ta_2O_5$-based ReRAM devices[J]. Nanoscale, 2016, 8(41): 17774-17781.

[78] Kim W, Menzel S, Wouters D J, et al. 3-bit multilevel switching by deep reset phenomenon in Pt/W/TaOX/Pt-ReRAM devices[J]. IEEE Electron Device Letters, 2016, 37(5): 564-567.

[79] Yihui Sun , Xiaoqin Yan, Xin Zheng , Yichong Liu, Yanwei Shen , and Yue Zhang. Influence of carrier concentration on the resistive switching characteristics of a ZnO-based memristor. Nano Research, 2016, 9: 1116-1124

[80] Sokolov A., Son S., Lim D., et al. Comparative study

of $Al_2O_3$, $HfO_2$, and $HfAlO_x$ for improved self-compliance bipolar resistive switching[J]. Journal of the American Ceramic Society, 2017, 100(12): 5638-5648.

[81] Ge N N, Gong C H, Yuan X C, et al. Effect of Mn doping on electroforming and threshold voltages of bipolar resistive switching in Al/Mn: NiO/ITO[J]. RSC advances, 2018, 8(52): 29499-29504.

[82] Li Y, Chu J, Duan W, et al. Analog and digital bipolar resistive switching in solution-combustion-processed NiO memristor. ACS Appl. Mater. Interfaces, 2018, 10（29）: 24598-24606

[83] Su Y T, Liu H W, Chen P H, et al. A method to reduce forming voltage without degrading device performance in hafnium oxide-based 1T1R resistive random access memory. IEEE J Electron Devi, 2018, 6: 341-345

[84] Chen S X, Chang S P, Chang S J, et al. Highly stable ultrathin $TiO_2$ based resistive random access memory with low operation voltage. Ecs J Solid State Sc, 2018, 7（7）: Q3183

[85] Chen S X, Chang S P, Hsieh W K, et al. Highly stable ITO/$Zn_2TiO_4$/Pt resistive random access memory and its application in two-bit-per-cell. RSC adv, 2018, 8（32）: 17622-17628

[86] Hu Q, Park M R, Abbas H, et al. Forming-free resistive switching characteristics in tantalum oxide and manganese oxide based crossbar array structure. Microelectronic Eng, 2018, 190: 7-10

[87]Wu Q, Banerjee W, Cao J, et al. Improvement of durability and switching speed by incorporating nanocrystals in the $HfO_x$ based resistive random access memory devices. Appl. Phys. Lett., 2018, 113（2）: 023105

[88] Ismail M, Nisa S U, Rana A M, et al. Enhancement of resistive switching performance by introducing a thin non-stoichiometric $CeO_{2-x}$ switching layer in $TiO_2$-based resistive random access memory[J]. Applied Physics Letters, 2019, 114(1).

[89] Tang L, Maruyama H, Han T, et al. Resistive switching in atomic layer deposited $HfO_2$/$ZrO_2$ nanolayer stacks[J]. Applied Surface Science, 2020, 515: 146015.

[90] Xing Li, Jian-Guo Yang, Hong-Ping Ma, Yu-Hang Liu, Zhi-Gang Ji, Wei Huang, Xin Ou, David Wei Zhang, and Hong-Liang Lu. Atomic Layer Deposition of Ga2O3/ZnO Composite Films for High-Performance Forming-Free Resistive Switching Memory. ACS Appl. Mater. Interfaces 2020, 12, 30538−30547

[91]Kempen T, Waser R, Rana V. 50x Endurance improvement in $TaO_x$ RRAM by extrinsic doping. 2021 IEEE International Memory Workshop （IMW）. New York: IEEE, 2021: 1-4

[92]Menzel S, Bengel C, Mohr J, et al. Reliability Aspects of Memristive Devices for Computation- in-Memory Applications[C]//2021 17th International Workshop on Cellular Nanoscale Networks and their Applications (CNNA). IEEE, 2021: 1-4.

[93] Song Y, Wang X, Wu Q, et al. High switching uniformity in HfOx-based memristors by adding polydopamine-derived Ag nanoparticles on the electrode. Appl. Phys. Lett., 2021, 118 (22):223501

[94] Guo T, Wang Y, Duan L, et al. Uniform switching behavior of $HfO_x$-based memory with gradual-grown filaments by interface modulation. Vacuum, 2021, 189: 110224.

[95] Ismail M, Abbas H, Sokolov A, et al. Emulating synaptic plasticity and resistive switching characteristics through amorphous $Ta_2O_5$ embedded layer for neuromorphic computing[J]. Ceramics International, 2021, 47(21): 30764-30776.

[96] Ismail M, Chand U, Mahata C, et al. Demonstration of synaptic and resistive switching characteristics in W/$TiO_2$/$HfO_2$/TaN memristor crossbar array for bioinspired neuromorphic computing. J Mater Sci Technol, 2022, 96: 94-102.

[97] Xu Y D, Jiang Y P, Tang X G, et al. Enhancement of resistive switching performance in Hafnium Oxide ($HfO_2$) devices via Sol-Gel method stacking tri-layer $HfO_2$/Al-ZnO/$HfO_2$ Structures. Nanomaterials, 2022, 13(1): 39-45

[98] Kim J, Park J, Kim S. Bipolar Switching characteristics

of transparent WOX-based RRAM for synaptic application and neuromorphic engineering. Materials, 2022, 15(20): 7185.
[99]Xu J, Qiao L, Yang Y, et al. $NbO_x$ RRAM Performance Enhancement by Surface Modification with Au Nanoparticles. Vacuum, 2024: 113422.
[100] Cui D, Lin Z, Kang M, et al. High performance low power multilevel oxide based RRAM devices based on $TiO_xN_y/Ga_2O_3$ hybrid structure[J]. Applied Physics Letters, 2024, 124(12).
[101] Micron MT29F4G08ABADAWP (4Gb SLC Parallel NAND Flash), [Online]. Available: https:// www.alldatasheet.com/.
[102] Winbond W25Q128JV (SPI NOR Flash), [Online]. Available: https:// www.alldatasheet.com/.
[103] G. Dong, Y. Xie, T. Zhang, and Y. Chen, Data Retention in MLC NAND Flash Memory: Characterization and Optimization, in Proceedings of the 50th Design Automation Conference (DAC), Austin, TX, USA, 2013, pp. 1-6, doi: 10.1145/2463209.2488798
[104] K. Kim, J. Choi, et al., A 90-nm 1.8-V 512-Mb NAND Flash Memory with 1.5-MB/s Program Throughput, IEEE Journal of Solid-State Circuits, vol. 40, no. 1, pp. 150-157, Jan. 2005. doi: 10.1109/JSSC.2004.837244.
[105] Kim S S, Yong S K, Kim W, et al. Review of semiconductor flash memory devices for material and process issues. Advanced Materials, 2023, 35(43): 2200659.